

Supporting information

Interfacial Gradient Engineering Synergized with Self-Adaptive Cathodic Defense for Durable Zn-Ion Batteries

Quan Zong <sup>a,b,c\*#</sup>, Xuelian Liu <sup>a#</sup>, Qilong Zhang <sup>b\*</sup>, Qiaoling Kang <sup>a</sup>, Fan Wang <sup>a</sup>, Guoying Wei <sup>a</sup>,  
Anqiang Pan <sup>c\*</sup>

<sup>a</sup> College of Materials and Chemistry, China Jiliang University, Hangzhou 310018, Zhejiang, People's Republic of China

<sup>b</sup> State Key Lab of Silicon and Advanced Semiconductor Materials, Zhejiang University, Hangzhou 310027, Zhejiang, People's Republic of China

<sup>c</sup> School of Materials Science & Engineering, Central South University, Changsha 410083, Hunan, People's Republic of China

\*Corresponding authors: E-mail: [quanzong@cjl.u.edu.cn](mailto:quanzong@cjl.u.edu.cn), [mse237@zju.edu.cn](mailto:mse237@zju.edu.cn),  
[pananqiang@csu.edu.cn](mailto:pananqiang@csu.edu.cn)

#These authors contributed equally to this work.

## **Experimental section**

### **Preparation of electrolytes**

The 2 M  $\text{ZnSO}_4$  was prepared by dissolving  $\text{ZnSO}_4 \cdot 7\text{H}_2\text{O}$  in deionized water. Different concentrations of diethyl phosphoramidate (0.05, 0.1, 0.2 M) were dissolved into 2 M  $\text{ZnSO}_4$  to obtain optimal electrolytes. All electrolytes were denoted as DP-0, DP-0.05, DP-0.1 and DP-0.2, respectively.

### **Preparation of $\text{NH}_4\text{V}_4\text{O}_{10}$**

0.468 g of  $\text{NH}_4\text{VO}_3$  and 0.604 g  $\text{H}_2\text{C}_2\text{O}_4 \cdot 2\text{H}_2\text{O}$  were dissolved in 80 mL of deionized water to form a homogenous solution. The mixture with a piece of carbon cloth was transferred to Teflon-lined autoclave and maintained at 180 °C for 6 h. After cooling, the precipitate and carbon cloth were washed with ethanol and deionized water several times and dried overnight at 80 °C. The  $\text{NH}_4\text{V}_4\text{O}_{10}$  powder, ketjen black, and polyvinylidene fluoride (PVDF) are mixed in ratio of 7:2:1 in the N-Methylpyrrolidone (NMP). The slurry was then coated uniformly on Ti foil and dried in a vacuum oven at 120 °C for 12 h.

### **Material characterizations**

Fourier transform infrared (FTIR, Thermo Fisher Scientific Nicolet iS20) spectra, Raman spectra (HORIBA HR Evolution) and Nuclear magnetic resonance (NMR, Bruker Avance III 400MHz) analysis were recorded to analyze the structure of electrolytes. Surface and chemical composition were analyzed via X-ray photoelectron spectroscopy (XPS, Thermo Scientific K-Alpha). The morphology of Zn deposition was characterized by scanning electron microscopy (SEM, Hitachi SU-4800) and 3D confocal laser scanning microscope (CLSM, KEYENCE VK-X150). The transmission electron microscope (TEM, JEM2100F) was employed to examine the structure of

SEI. The pH values of the electrolytes were recorded on a pH meter (PHS-25). The crystal structure was investigated using an X-ray diffractometer (XRD, Bruker D8 Discover X). Contact angle measurements were recorded using a contact angle meter (Dataphysics OCA20). The viscosity of electrolyte was recorded by Rotary Viscometer (brookfield DV-2 pro).

### **Electrochemical measurements**

CV curves of the symmetric cells were collected on an electrochemical workstation (CHI 760e, Chenhua) within a voltage range of  $-15$  mV to  $15$  mV at different scan rates for the electric double layer capacitance (EDLC) measurements. CV curves of Zn||Ti asymmetric cells were collected within a voltage range of  $-0.2$  V to  $0.5$  V at a scan rate of  $1$  mV  $s^{-1}$ . CV tests were conducted in the voltage range of  $0.2$ – $1.6$  V for full cells. ACV measurement of Zn||Cu asymmetric cells was tested in the voltage range of  $0$  to  $1$  V at  $1$  mV  $s^{-1}$ . The Tafel and linear sweep voltammetry (LSV) curves were acquired via a three-electrode cell at a scan rate of  $1$  mV  $s^{-1}$ , with Zn foil as the working electrode, Pt as the counter electrode, and Ag/AgCl as the reference electrode. Chronoamperometry (CA) curves were obtained under an overpotential of  $-150$  mV. Electrochemical impedance spectroscopy (EIS) were collected with the frequency of  $0.1$  Hz to  $100$  kHz. The Zn||Zn symmetric cells, Zn||Cu symmetric cells and Zn||NVO full cells were assembled in the coin cells (CR2032). The cycling performance was measured using a NEWARE battery test system (CT-4008, Shenzhen, China) at  $30$  °C.

The ionic conductivity ( $\sigma$ ) was estimated based on equation:

$$\sigma = \frac{L}{RS}$$

where R is the resistance, S is the area, and L is the thickness of the SEI layer.<sup>1</sup>

The EDLC was calculated by the following equation:

$$C = \frac{i_c}{v}$$

where  $i_c$  refers to the half value of current difference during positive scan and negative scan at 0 V, and  $v$  refers to the scan rates.<sup>2</sup>

$Zn^{2+}$  transference number was calculated according to

$$t_{Zn^{2+}} = \frac{I_s(\Delta V - I_0 R_0)}{I_0(\Delta V - I_s R_s)}$$

where  $\Delta V$  is the applied voltage of the polarization tests (10 mV),  $I_0$  and  $R_0$  are the initial current and resistance, and  $I_s$  and  $R_s$  are the steady-state current and resistance, respectively.<sup>3</sup>

The activation energy could be evaluated by the Arrhenius equation:

$$\frac{1}{R_{ct}} = A \exp\left(\frac{-E_a}{RT}\right)$$

where  $R_{ct}$  is the charge-transfer resistance,  $A$  is the frequency factor,  $R$  is the ideal gas constant, and  $T$  is the absolute temperature.<sup>4</sup>

### Theoretical calculations

All the DFT calculations were conducted based on the Vienna Ab initio Simulation Package (VASP).<sup>5</sup> The exchange-correlation potential was described by the Perdew–Burke–Ernzerhof (PBE) generalized gradient approach (GGA).<sup>6</sup> The electron-ion interactions were accounted by the projector augmented wave (PAW).<sup>7</sup> All DFT calculations were performed with a cut-off energy of 400 eV, and the Brillouin zone was sampled with a  $3 \times 3 \times 1$  k-point grid. The energy and force convergence criteria of the self-consistent iteration were set to  $10^{-5}$  eV and  $0.02 \text{ eV \AA}^{-1}$ , respectively. Besides, the DFT + U correction for V atoms was taken into account, and the U-J value of 4.0 for V. DFT-D3 method was used to describe van der Waals (vdW) interactions.<sup>8</sup> VESTA software was used to visualize the results.<sup>9</sup>

The adsorption energy ( $E_{ads}$ ) of adsorbate A was defined as

$$E_{\text{ads}} = E_{\text{A}}^* - E_{\text{A}} - E_{\text{sub}}$$

where  $E_{\text{A}}^*$  represent the energy of A adsorbed on the surface.  $E_{\text{sub}}$  is the energy of clean surface,  $E_{\text{A}}$  represent the energies of A molecule.

HOMO-LUMO energy levels were investigated with the Gaussian 16 software package. Structural optimization and electronic properties calculations were performed using the B3LYP functional with the def2-TZVP basis set (empirical dispersion correction GD3(BJ)). Calculations of frequency were accomplished at the parallel level of the theory (no imaginary frequency) to confirm the optimized-geometries as true minima. The aqueous environment was simulated using SMD model.<sup>10</sup>

Quantum chemistry (QC) calculation was performed with a Gaussian16 software to investigate the interaction between ions or molecules. B3LYP functional was used as it is robust for both main group elements and transition elements. GD3(0) dispersion correction was used to improve the precision of weak interactions. 6-311+G (d, p) basis set was used for C, H, O, N, S and P atoms while Lanl2TZ basis set was used for Zn atoms. The restrained electrostatic potential (RESP) atom charges and electrostatic potential (ESP) were calculated through Multiwfn software.<sup>11</sup> Molecular dynamics (MD) simulation was performed through Gromacs2022.1 software to study the bulk electrolyte solvation.<sup>12</sup> The force field parameters of  $\text{Zn}^{2+}$  ions and TIP3P water model was obtained with Amber99SB force field. The GAFF force field parameters of DP,  $\text{SO}_4^{2-}$  molecules were generated with Acyppe program. RESP atom charges were used to describe electrostatic interactions. Atomic charges of all ions were multiplied by scale factor 0.70 to correct the polarization effect of ions.

The boxes of electrolyte were built by filling molecules randomly. The equilibrium simulation

was carried out with NPT ensemble at 298 K and 1 bar for 500 ps. The production simulation was carried out with NPT ensemble at 298 K for 20 ns. The distribution of number density was calculated through Gromacs2022.1. VMD software was used to visualize the systems and obtain the ion association state.

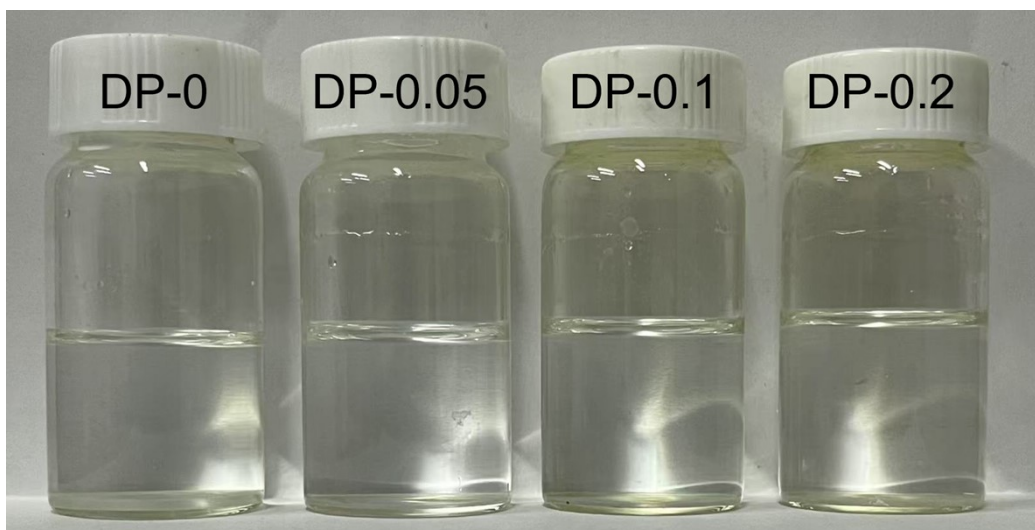


**Fig. S1** Optical photographs of ZnSO<sub>4</sub> electrolytes with different concentrations of DP.

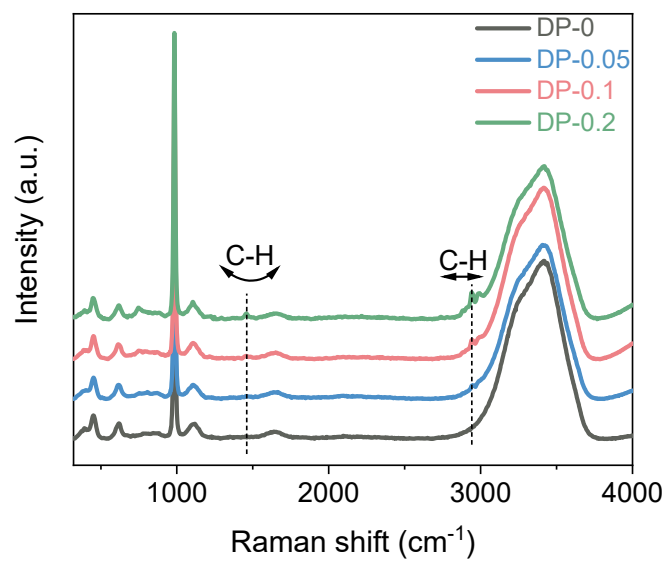


**Fig. S2** Raman spectra of different electrolytes.

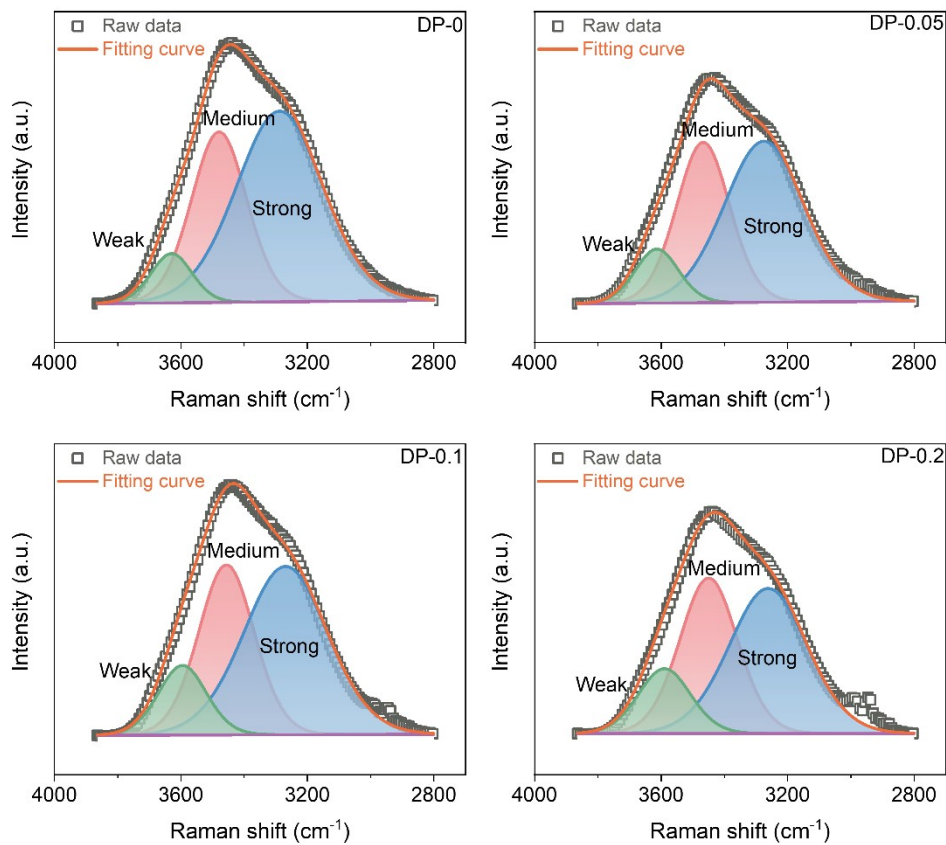


**Fig. S3** The fitted O-H stretching consists of strong, weak, and medium H-bonds.

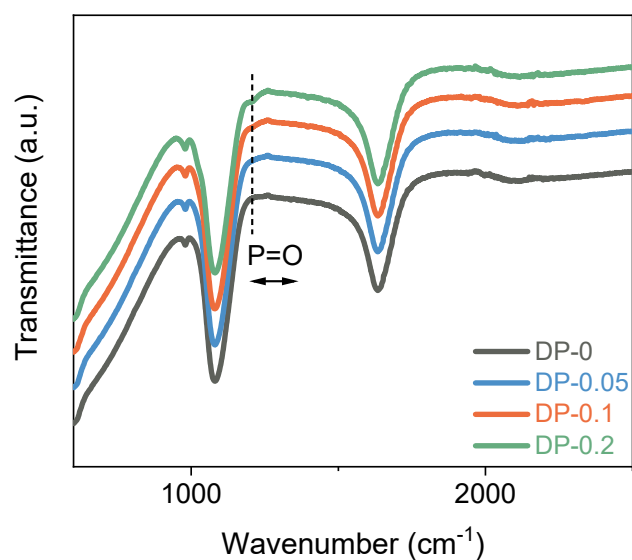


**Fig. S4** FTIR spectra of different electrolytes.

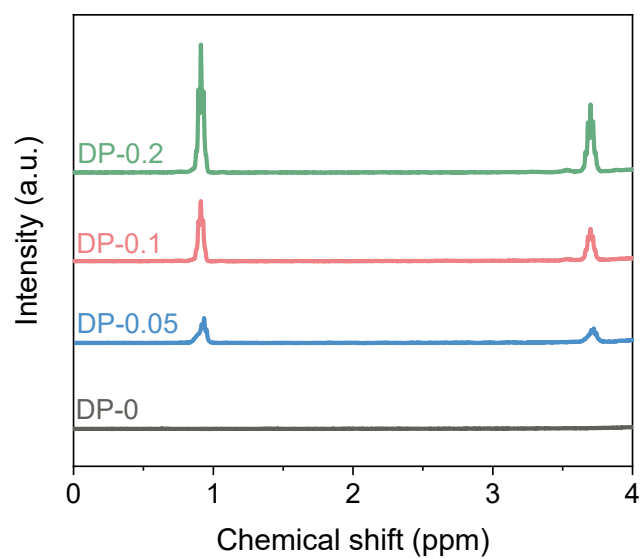


**Fig. S5** NMR spectra of different electrolytes.

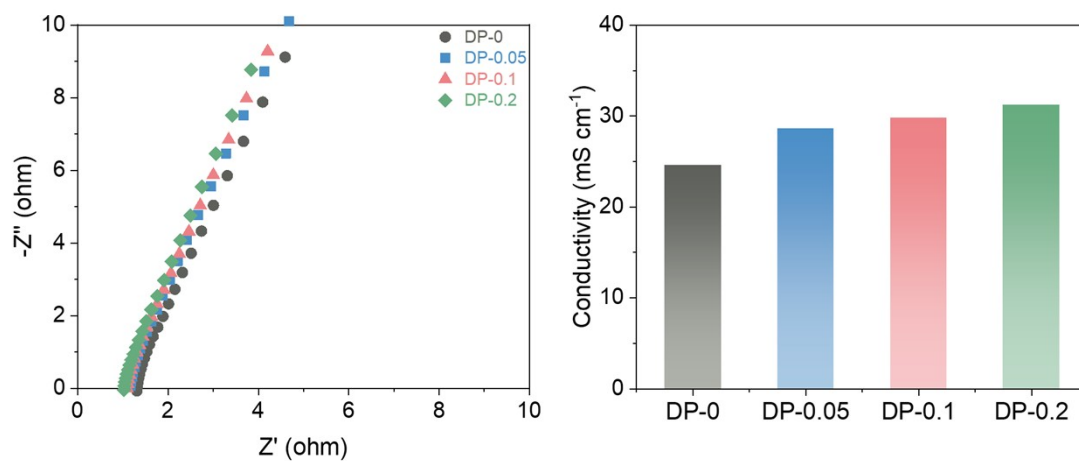


**Fig. S6** Ionic conductivities of different electrolytes.

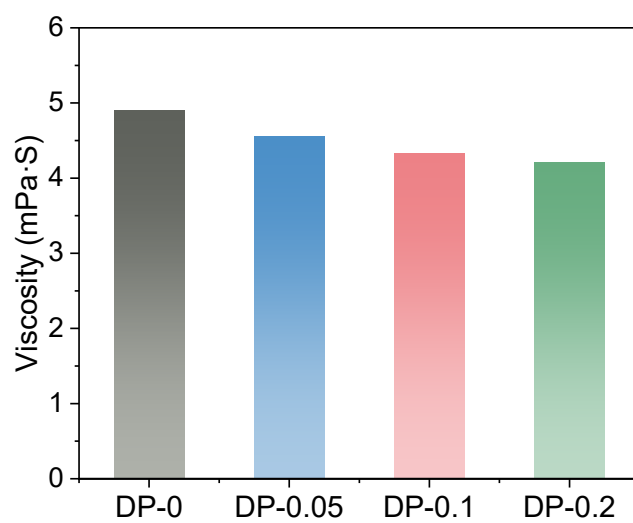


**Fig. S7** Viscosity of different electrolytes.

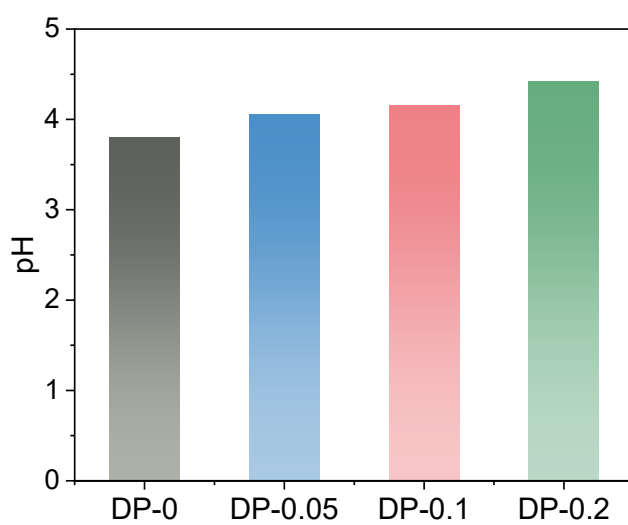


**Fig. S8** pH values of different electrolytes.

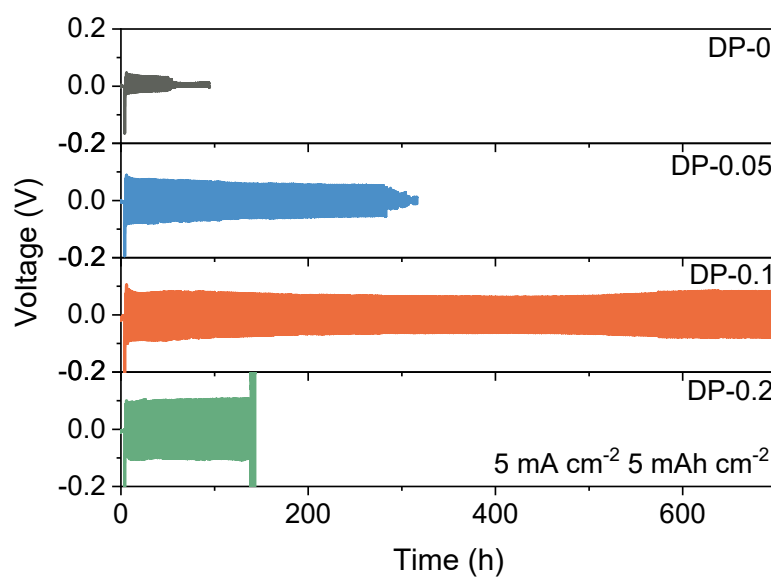


**Fig. S9** Cycling performance of Zn||Zn symmetric cells with different electrolytes at  $5 \text{ mA cm}^{-2}$  and  $5 \text{ mAh cm}^{-2}$ .

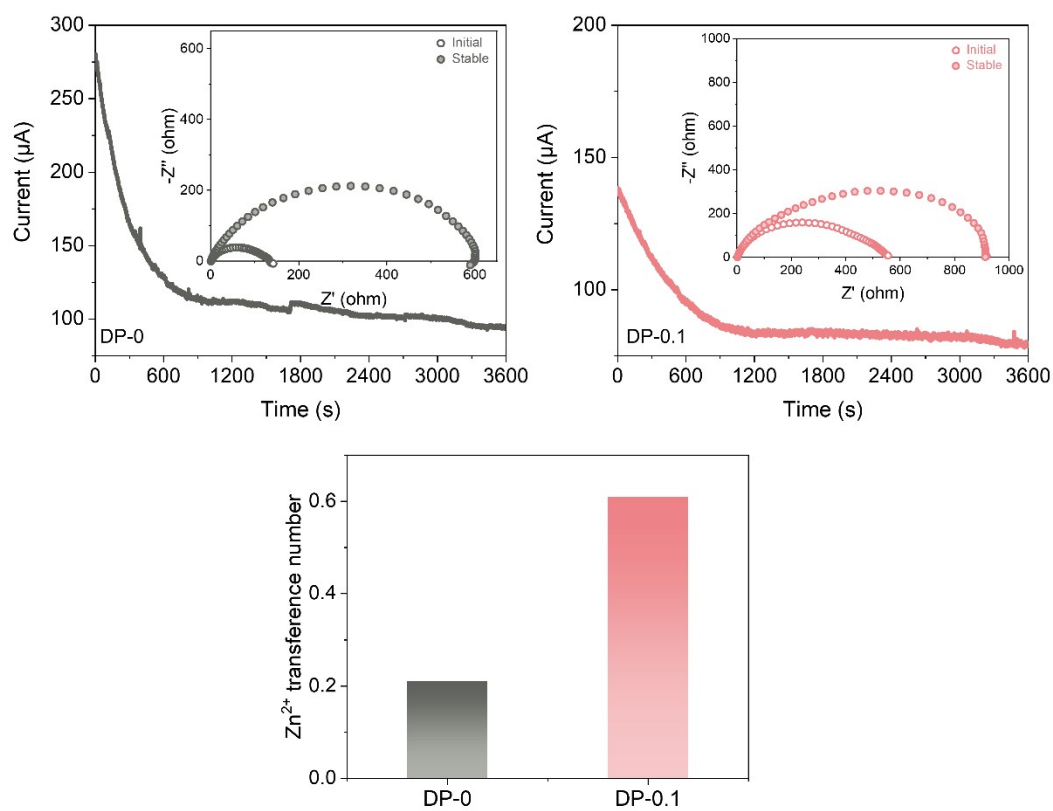


**Fig. S10** Zn<sup>2+</sup> transference number in DP-0 and DP-0.1.

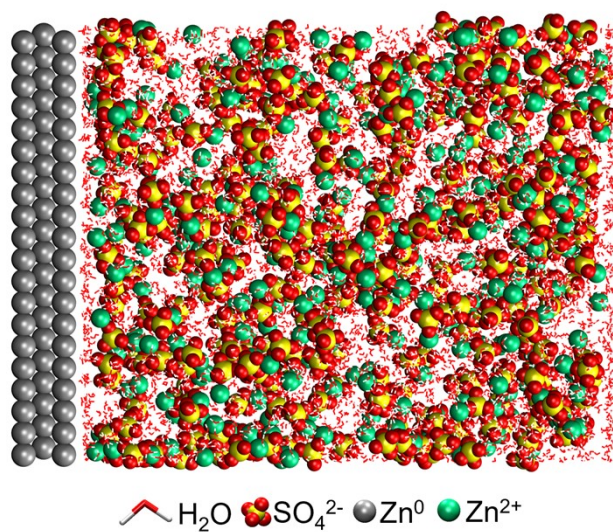


**Fig. S11** MD simulations of the interface region in DP-0 system.

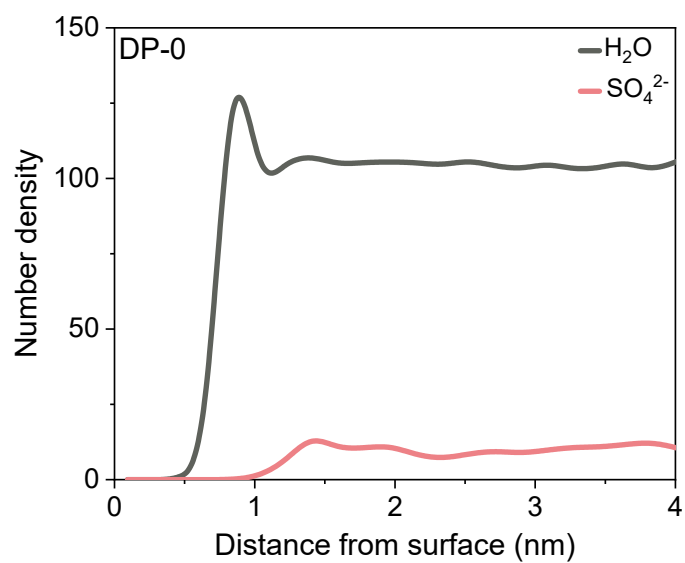


**Fig. S12** Relative concentration distribution of H<sub>2</sub>O and SO<sub>4</sub><sup>2-</sup> species in the interface region in DP-0 electrolyte.

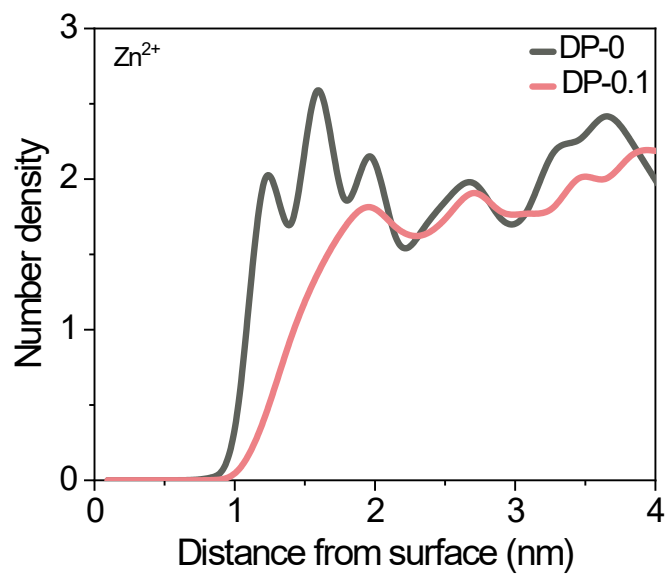


**Fig. S13** Relative concentration distribution of  $Zn^{2+}$  in the interface region in DP-0 and DP-0.1 electrolytes.

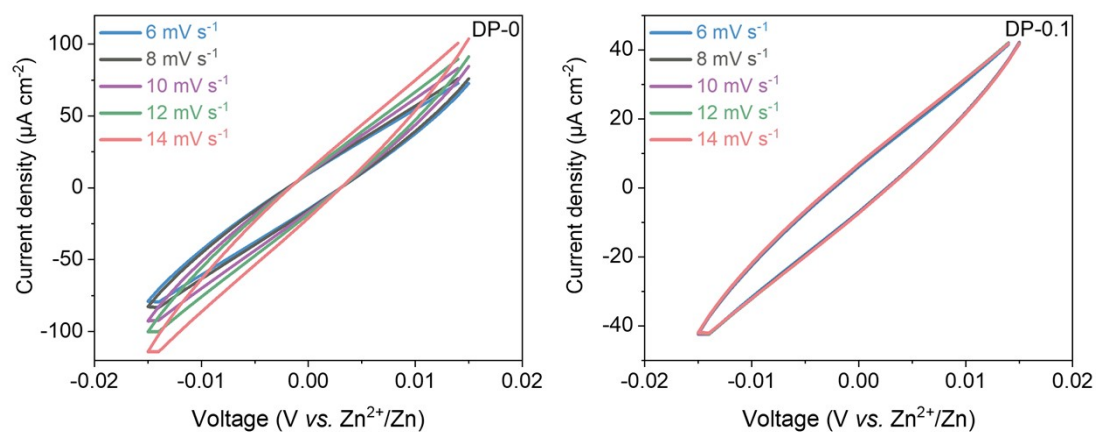


**Fig. S14** CV curves in the Zn||Zn symmetric cells with DP-0 and DP-0.1 electrolytes.

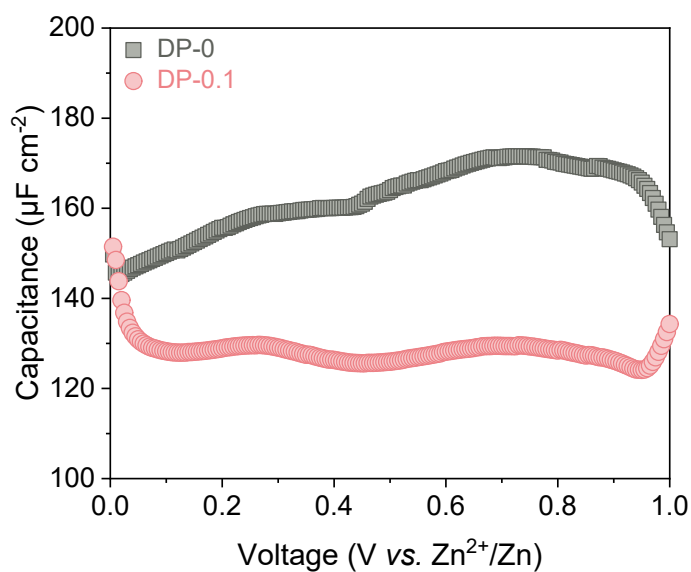


**Fig. S15** ACV curves of Zn||Cu asymmetric cells with DP-0 and DP-0.1 electrolytes.

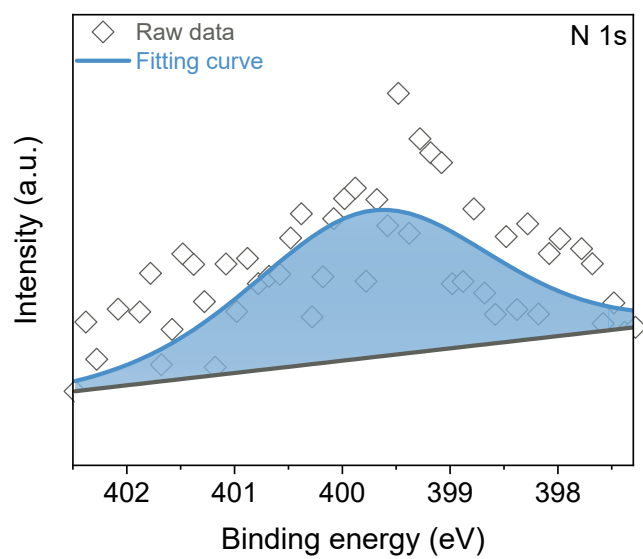


**Fig. S16** N 1s XPS spectra of immersed Zn foils in DP-0.1 electrolyte.

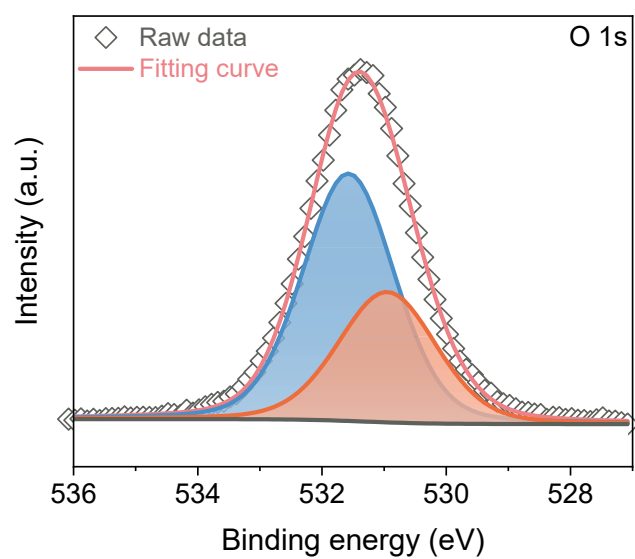


**Fig. S17** O 1s XPS spectra of immersed Zn foils in DP-0.1 electrolyte.

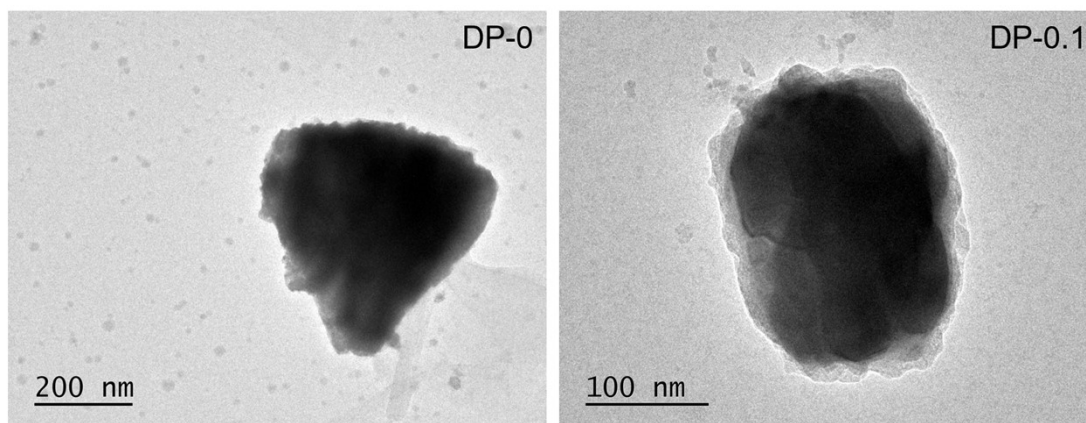


**Fig. S18** TEM images of deposited Zn in DP-0 and DP-0.1 electrolytes.

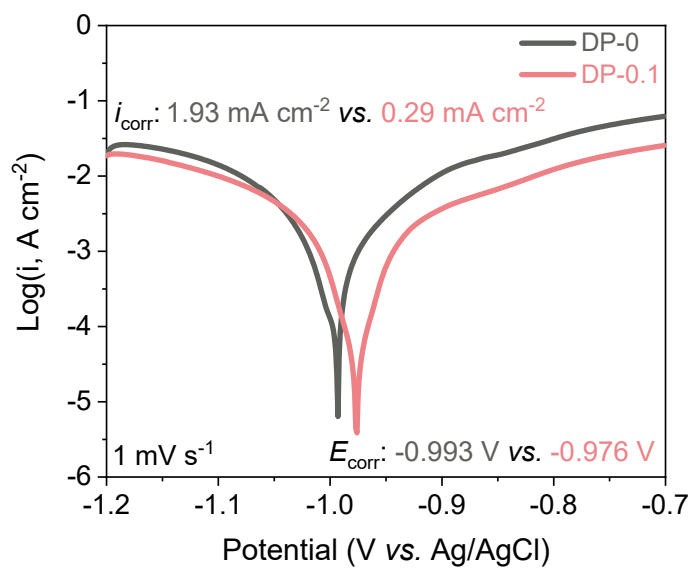


**Fig. S19** Tafel curves of Zn anodes in DP-0 and DP-0.1 electrolytes.

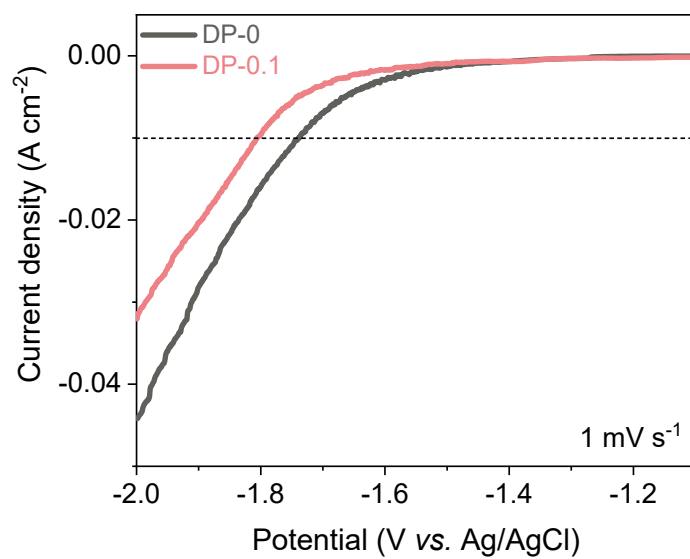


**Fig. S20** LSV curves of Zn anodes in DP-0 and DP-0.1 electrolytes.

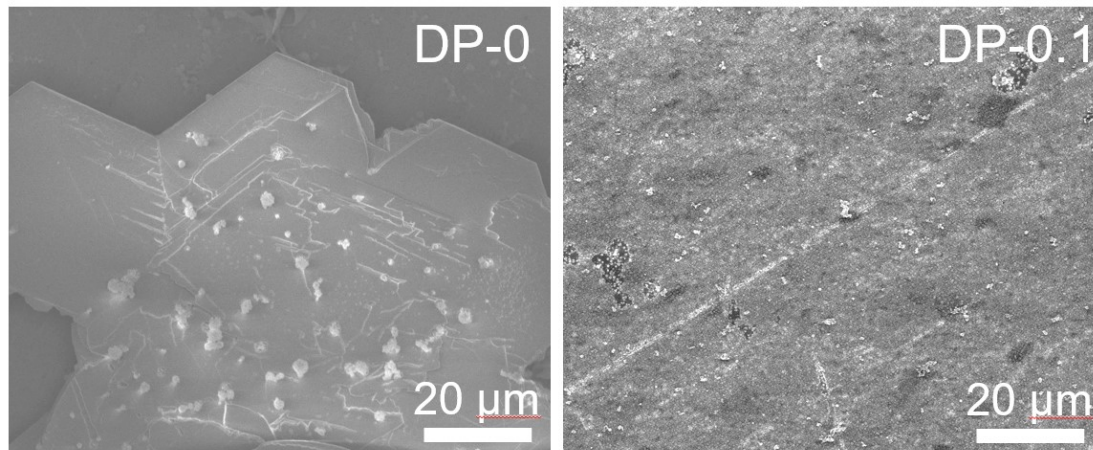


**Fig. S21** SEM images of Zn foils immersed in DP-0 and DP-0.1 electrolytes.

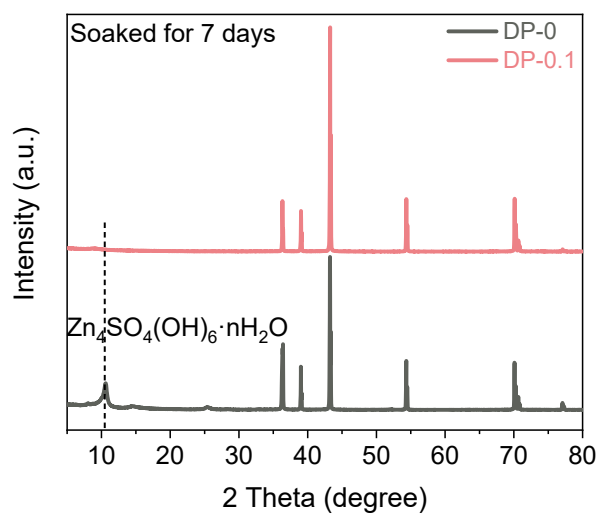


**Fig. S22** XRD patterns of Zn foils immersed in DP-0 and DP-0.1 electrolytes.

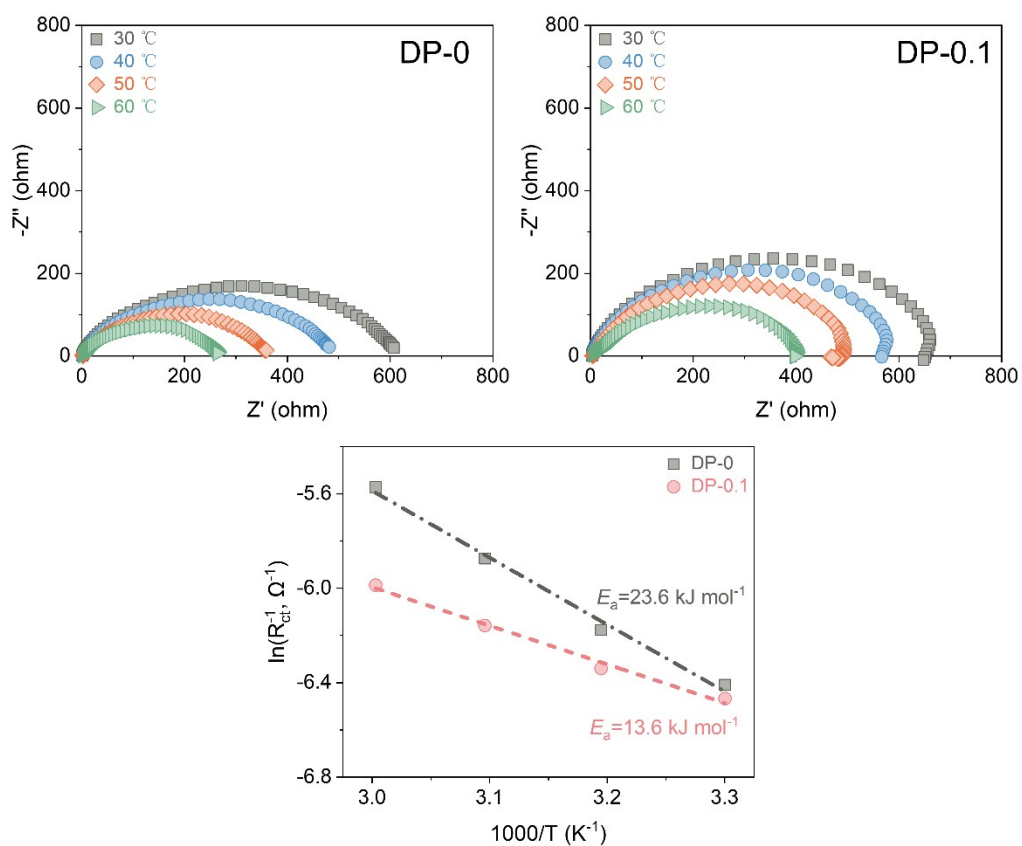


**Fig. S23** EIS plots of Zn||Zn symmetric cells with DP-0 and DP-0.1 electrolytes and the fitted  $E_a$ .

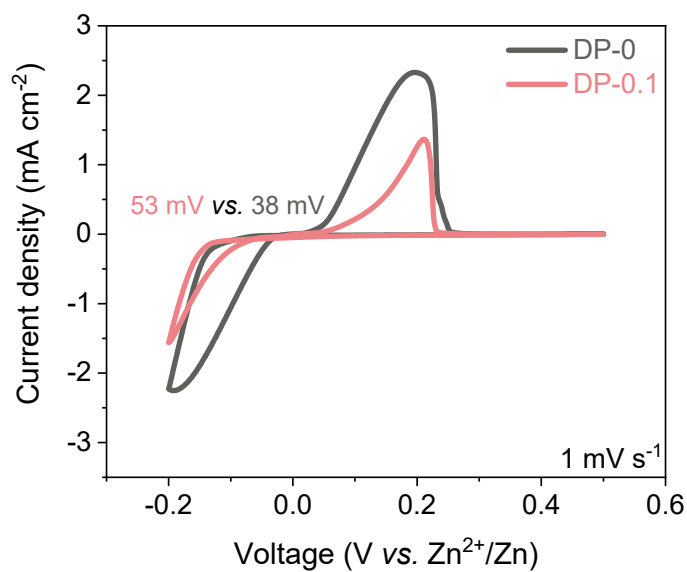


**Fig. S24** CV curves of Zn||Ti cells with DP-0 and DP-0.1 electrolytes.

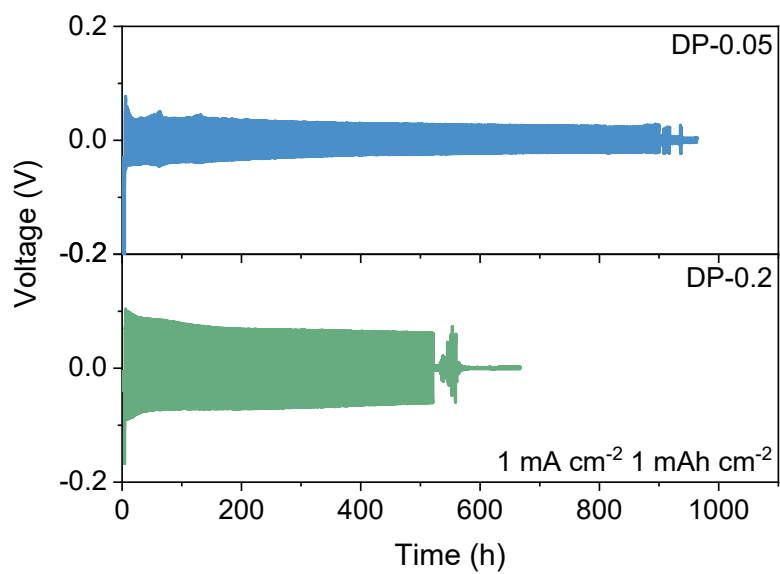


**Fig. S25** Cycling performance of Zn||Zn symmetric cells with DP-0.05 and DP-0.2 electrolytes.

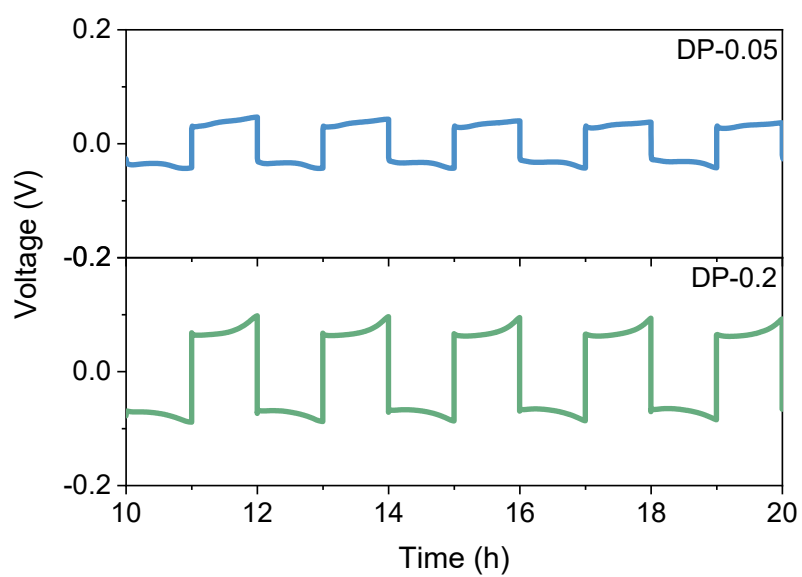


**Fig. S26** Voltage profiles of Zn||Zn symmetric cells with DP-0.05 and DP-0.2 electrolytes.

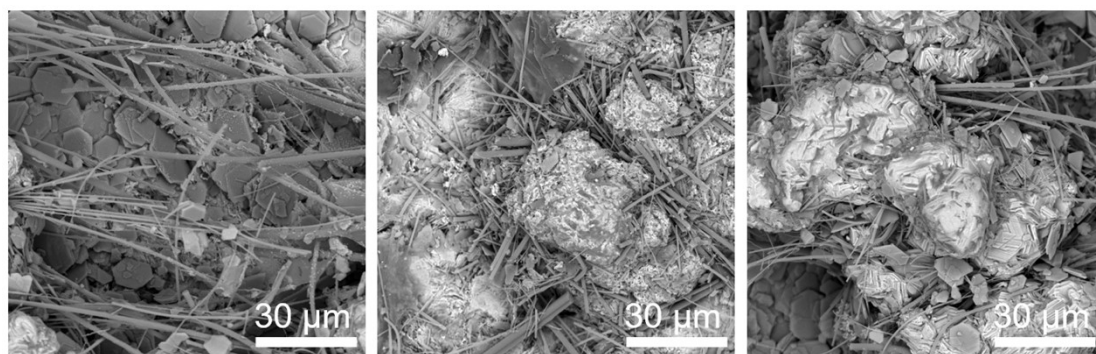


**Fig. S27** SEM images of Zn anodes cycled in DP-0 electrolyte after different cycles.

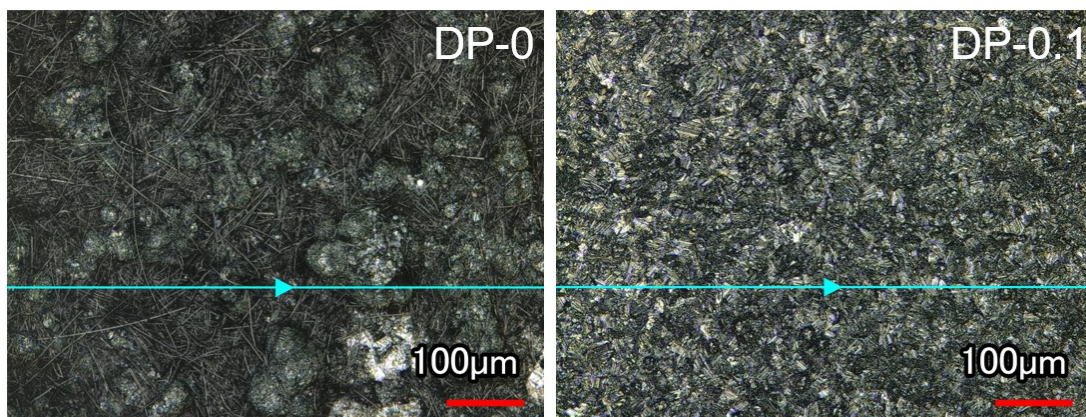


**Fig. S28** CLSM images of deposited Zn in different electrolytes.

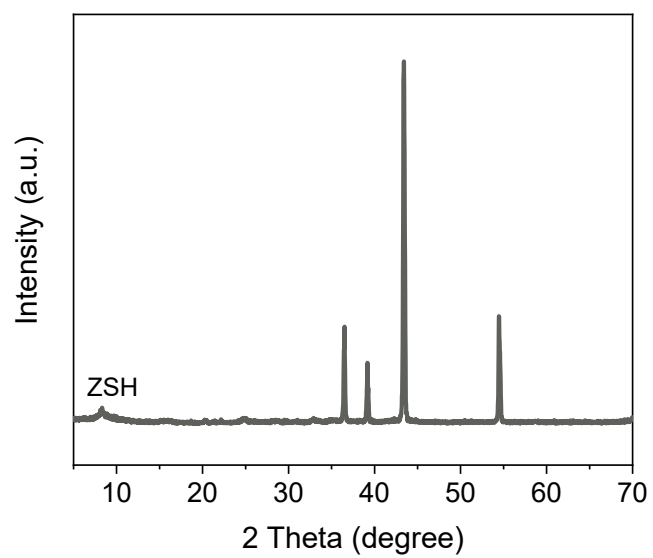


**Fig. S29** XRD pattern of Zn cycled in DP-0.

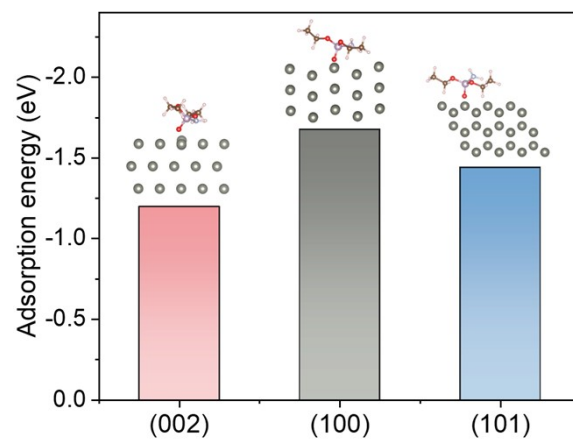


**Fig. S30** The adsorption energies of DP on different crystal planes of Zn anode.

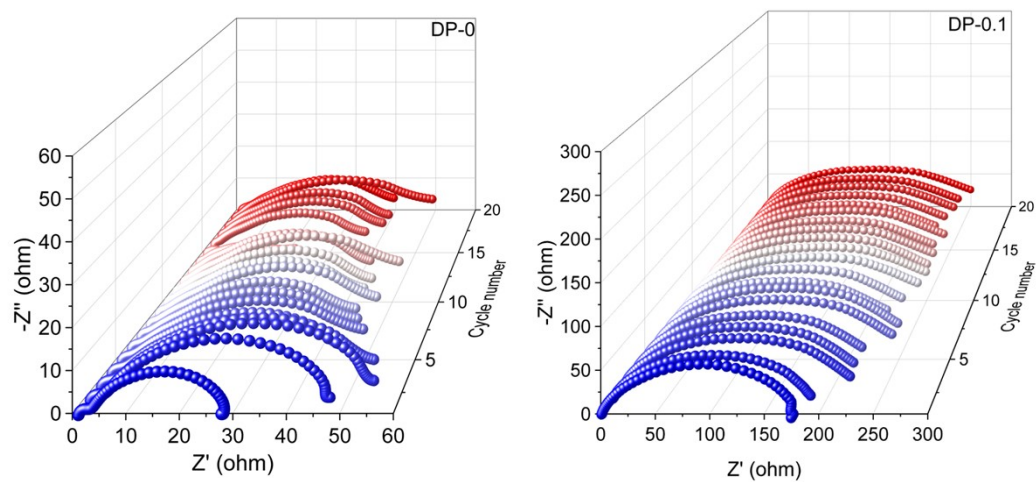


**Fig. S31** In situ EIS plots of Zn||Zn symmetric cells with different electrolytes.

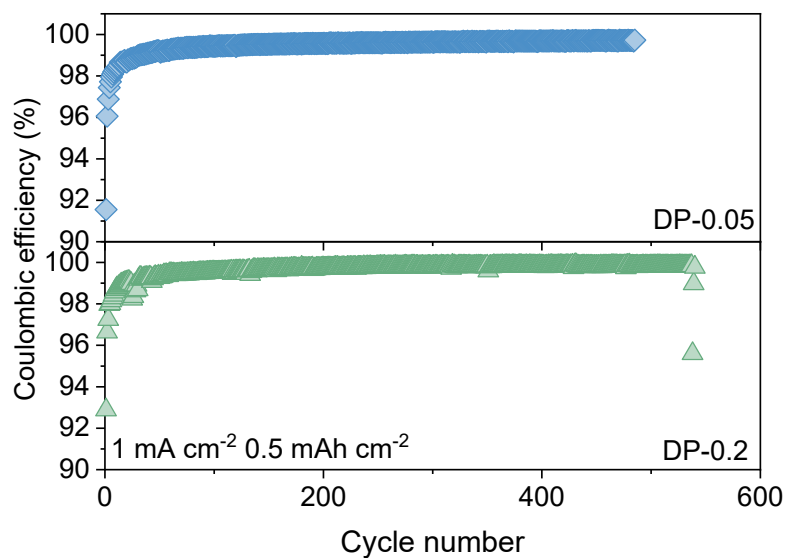


**Fig. S32** Cycling performance of Zn||Cu asymmetric cells with DP-0.05 and DP-0.2 electrolytes.

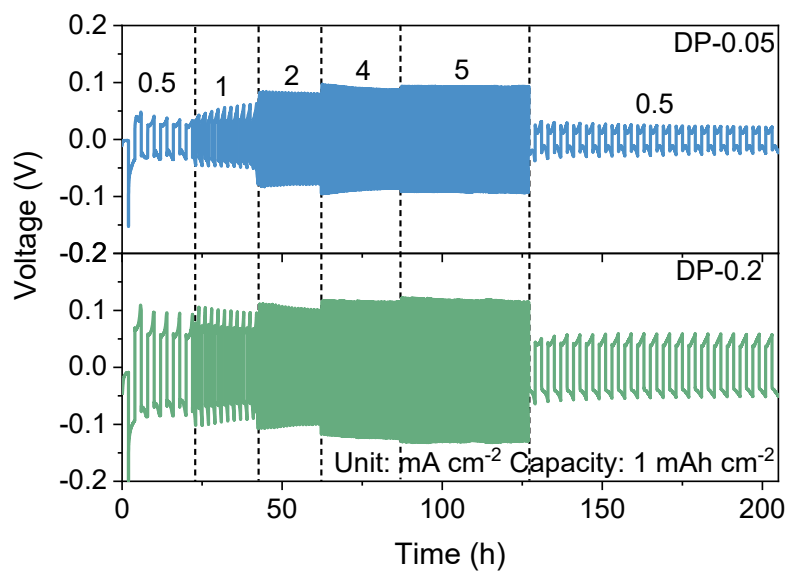


**Fig. S33** Rate performance of symmetric cells at different current densities with 1 mAh cm<sup>-2</sup>.

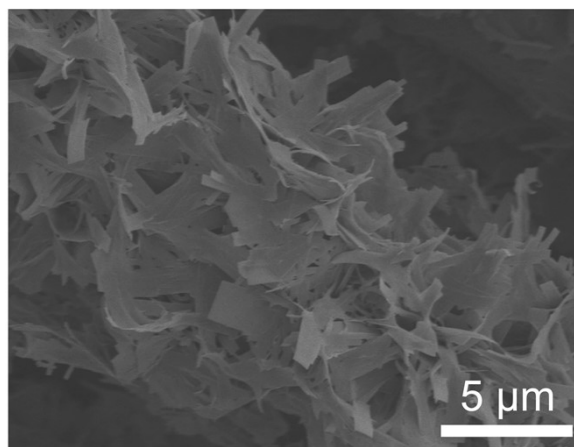


**Fig. S34** SEM image of NVO.

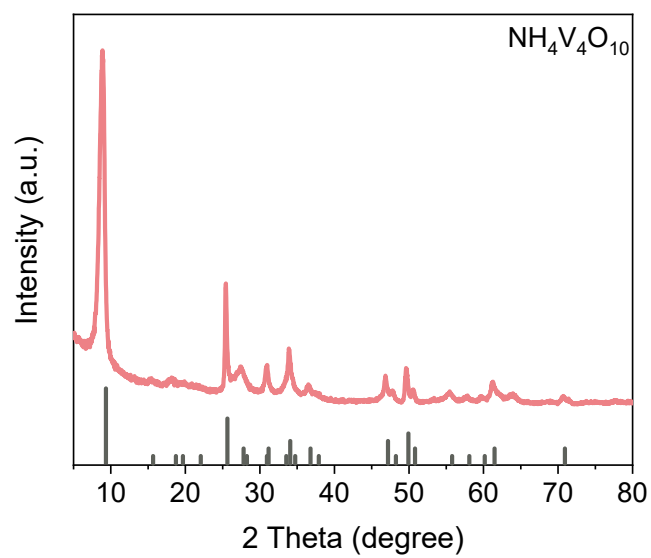


**Fig. S35** XRD pattern of NVO.

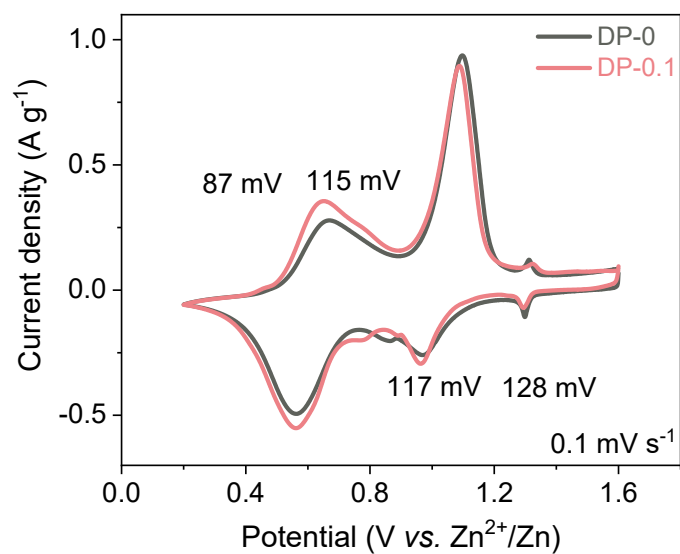


**Fig. S36** CV curves at 0.1 mV s<sup>-1</sup>.

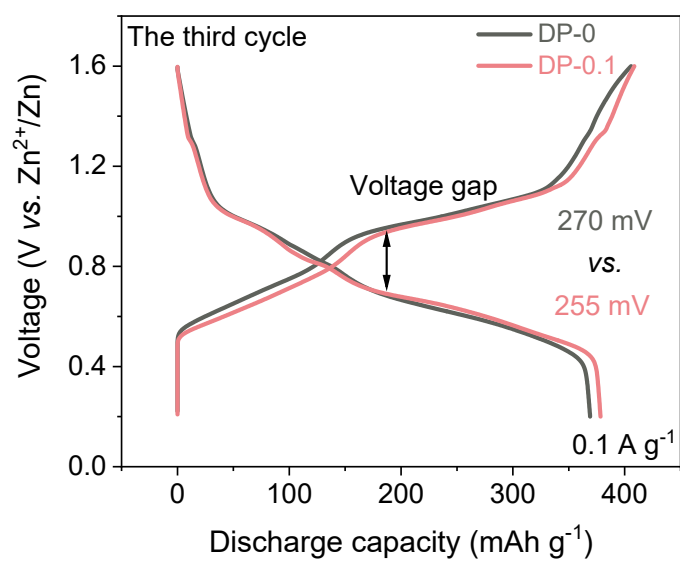


**Fig. S37** GCD curves at 0.1 A g<sup>-1</sup>.

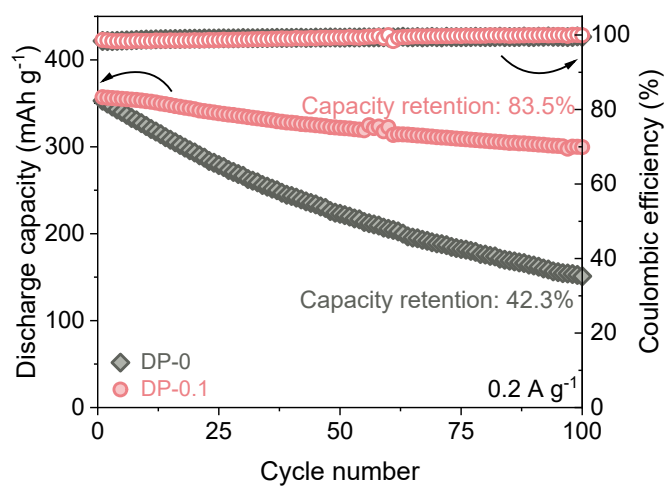


**Fig. S38** Cycling performance of Zn||NVO using DP-0 and DP-0.1 electrolytes at 0.2 A g<sup>-1</sup>.

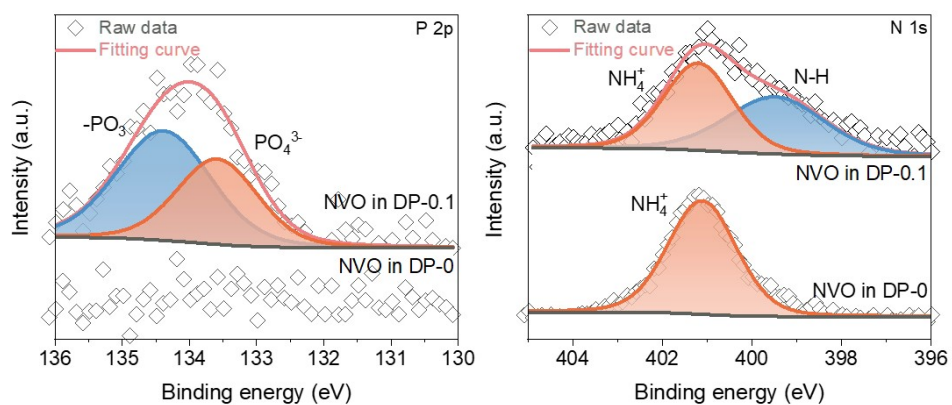


**Fig. S39** P2p and N 1s XPS spectra of NVO cycled in DP-0 and DP-0.1 electrolytes.

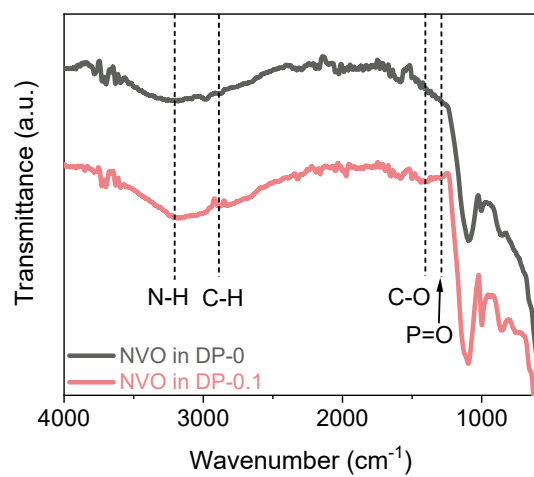


**Fig. S40** FTIR spectra of NVO cycled in DP-0 and DP-0.1 electrolytes.

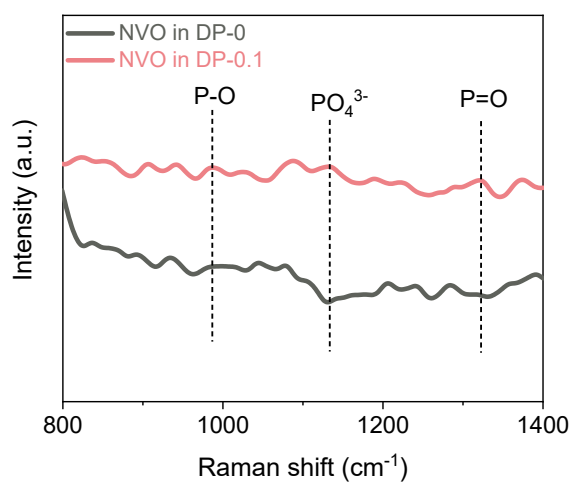


**Fig. S41** Raman spectra of NVO cycled in DP-0 and DP-0.1 electrolytes.

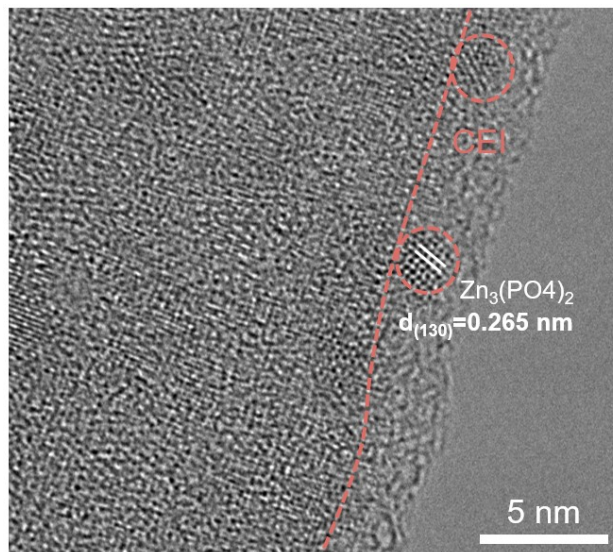


**Fig. S42** HRTEM image of NVO cycled in DP-0.1 electrolyte.



**Fig. S43** Optical photograph of electrodes immersed in DP-0 and DP-0.1 electrolytes.

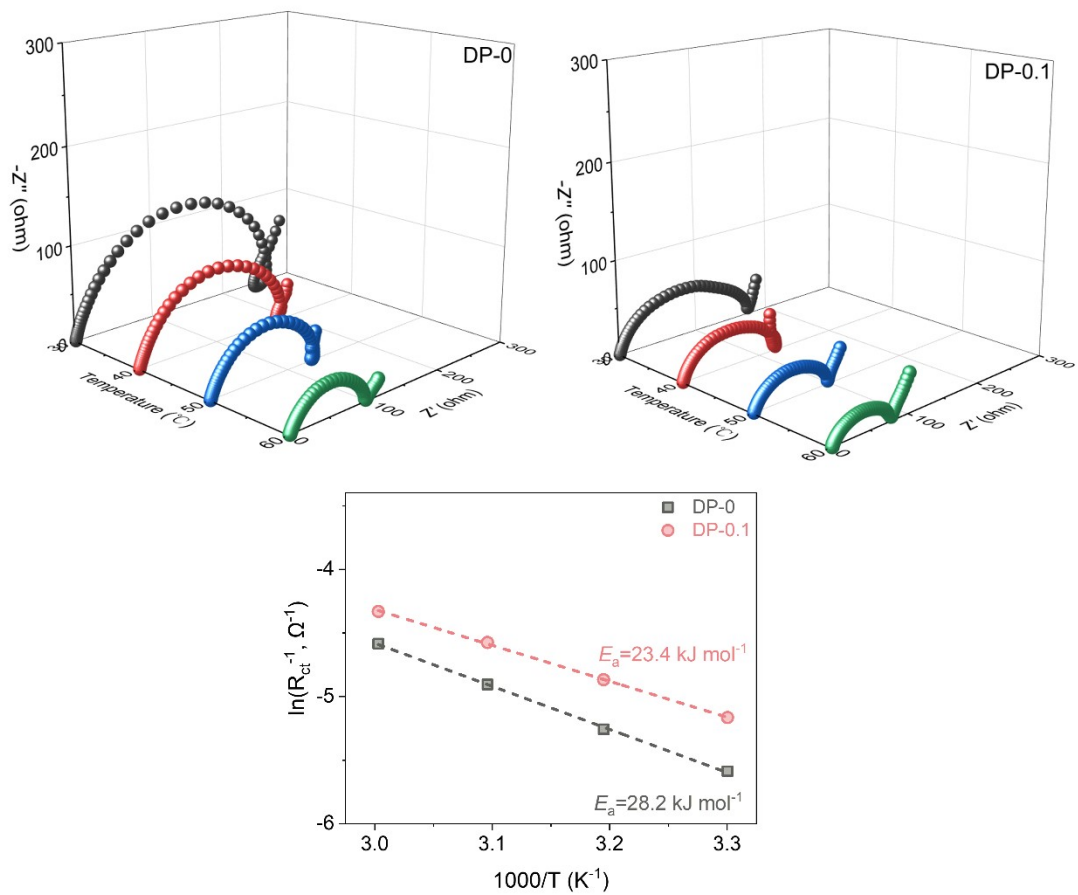


**Fig. S44** EIS plots of Zn||NVO cells with DP-0 and DP-0.1 electrolytes and the fitted  $E_a$ .

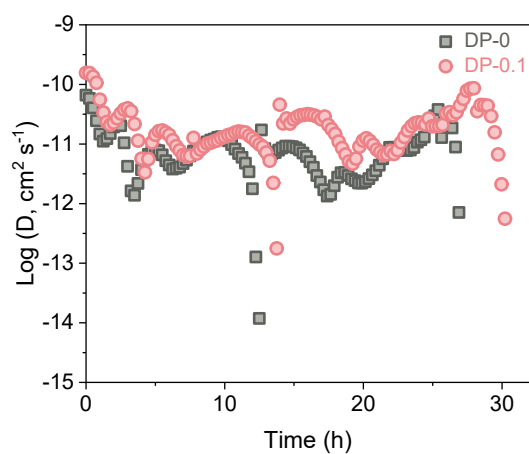


**Fig. S45** GITT curves and  $D_{\text{Zn}^{2+}}$  of the Zn||NVO full cells with/without DP additive.

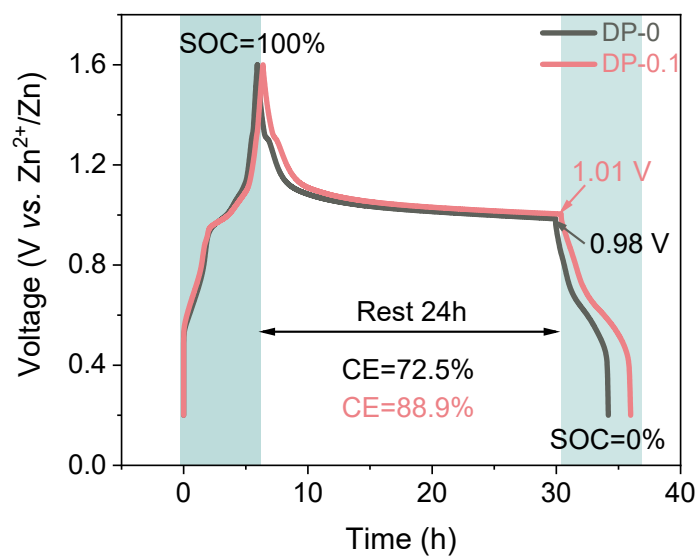


**Fig. S46** Self-discharge behavior of full cell with DP-0 and DP-0.1 electrolytes.

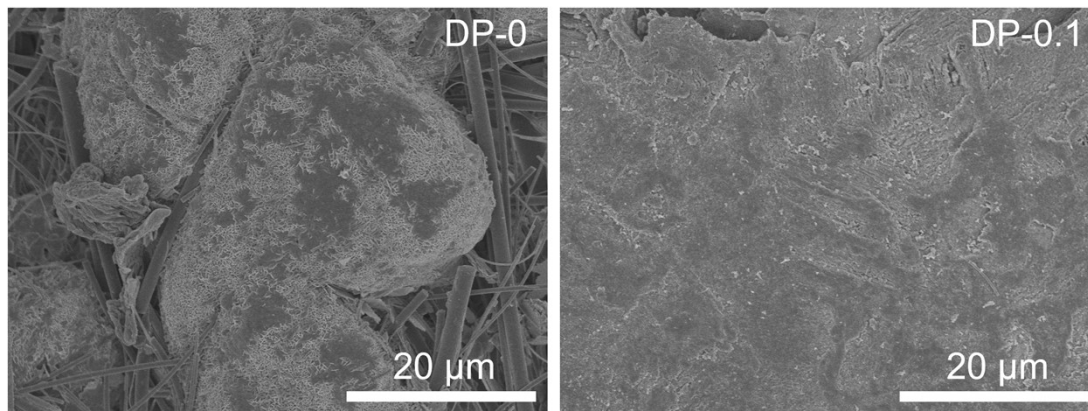


**Fig. S47** SEM images of Zn anode after cycling in the full cells.

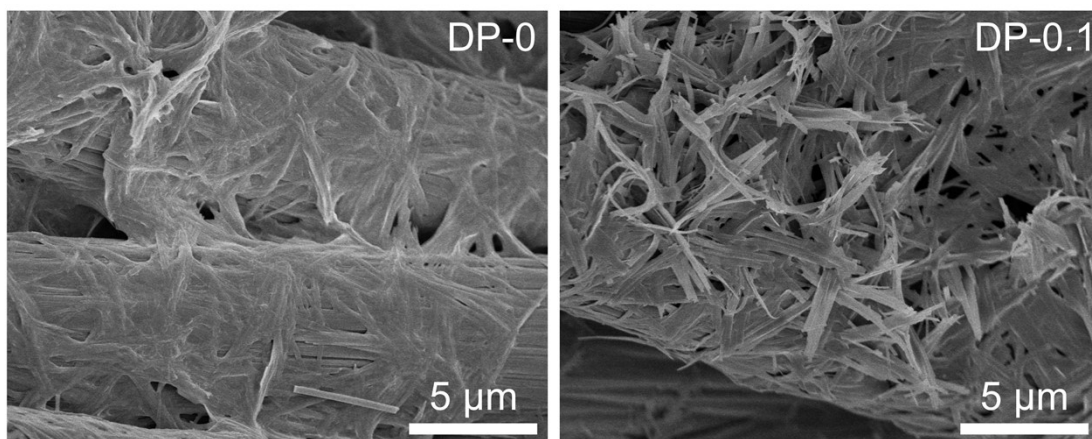


**Fig. S48** SEM images of NVO after cycling in the full cells.

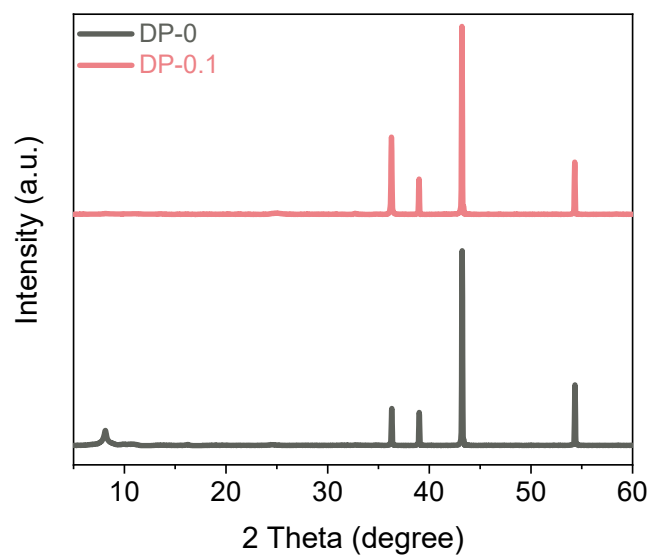


**Fig. S49** XRD patterns of Zn anode after cycling in the full cells.

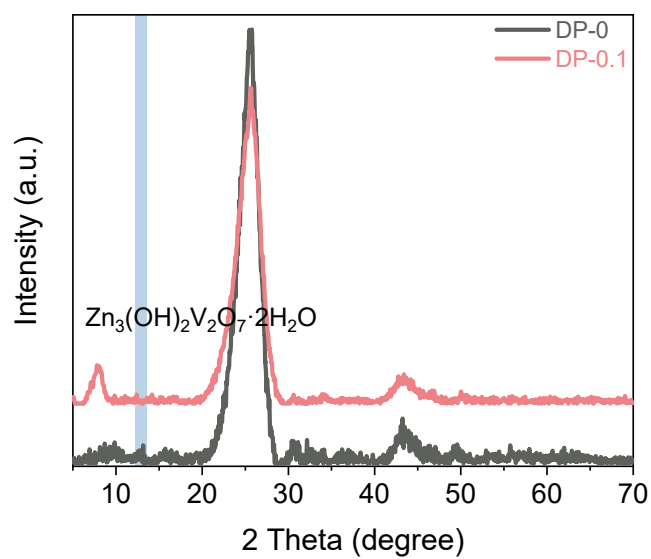


**Fig. S50** XRD patterns of NVO after cycling in the full cells.

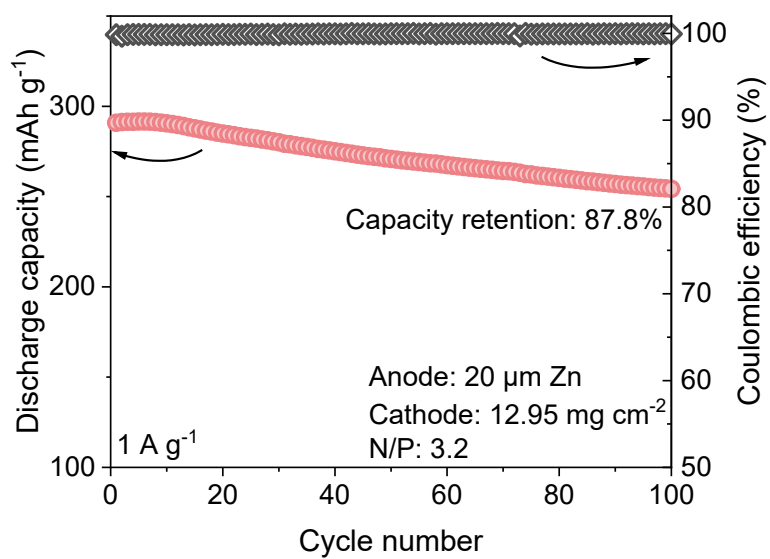


**Fig. S51** Cycling performance of Zn||NVO pouch cell with a N/P ratio of 3.2.

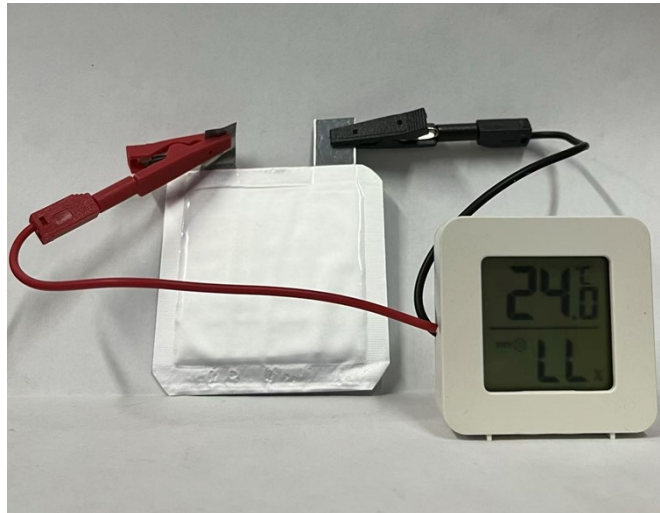


**Fig. S52** Optical photo of the pouch cell powering a thermometer.

**Table S1.** Comparison of the electrochemical properties of cells using DP with other additives.

Additives	Current density (mA cm <sup>-2</sup> )	Areal capacity (mAh cm <sup>-2</sup> )	Cycling life (h)	Average CE (%)	Ref.
DP	1	1	2200	99.7	This work
	10	5	1200		
NMU	10	1	1600	99.7	13
PA	1	1	1800	—	14
	2	2	1200		
TEP, DMSO	5	1	800	99.4	15
EC	1	1	750	98.8	16
18-crown-6	10	2	1300	—	17
Capping agent	1	1	2000	99.2	18
	5	5	900		
LBG	1	1	1600	99.6	19
FCD	5	5	800	99.5	20
PDMAPS	3	3	800	99.3	21
LPL	1	1	1500	99.5	22
LA	1	1	2200	99.3	23
	10	10	800		
Cor	5	5	900	99.5	24

## References

1. H. Jia, X. Jiang, Y. Wang, Y. Lam, S. Shi and G. Liu, *Adv. Energy Mater.*, 2024, **14**, 2304285.
2. P. Wang, H. Zhou, Y. Zhong, X. Sui, G. Sun and Z. Wang, *Adv. Energy Mater.*, 2024, **14**, 2401540.
3. C. Chang, S. Hu, T. Li, F. Zeng, D. Wang, S. Guo, M. Xu, G. Liang, Y. Tang, H. Li, C. Han and H.-M. Cheng, *Energy Environ. Sci.*, 2024, **17**, 680-694.
4. T. Long, Q. Y. Zhao, G. Y. Yin, P. X. Xie, S. Liu, X. Ma, Q. Wu, B. Y. Lu, Z. Dai and X. X. Zeng, *Adv. Funct. Mater.*, 2024, **34**, 2315539.
5. G. Kresse and J. Hafner, *Phys. rev. B*, 1993, **47**, 558.
6. J. P. Perdew, K. Burke and M. Ernzerhof, *Phys. rev. lett.*, 1996, **77**, 3865.
7. G. Kresse and D. Joubert, *Phys. rev. b*, 1999, **59**, 1758.
8. S. Grimme, J. Antony, S. Ehrlich and H. Krieg, *J. Chem. Phys.*, 2010, **132**.
9. K. Momma and F. Izumi, *Appl. Crystallography*, 2011, **44**, 1272-1276.
10. A. V. Marenich, C. J. Cramer and D. G. Truhlar, *J. Phys. Chem. B*, 2009, **113**, 6378-6396.
11. T. Lu and F. Chen, *J. Computat. Chem.*, 2012, **33**, 580-592.
12. D. Van Der Spoel, E. Lindahl, B. Hess, G. Groenhof, A. E. Mark and H. J. Berendsen, *J. Computat. Chem.*, 2005, **26**, 1701-1718.
13. W. Zhang, R. Chen, Y. Dai, X. Wu, J. Chen, W. Zong, M. Zhang, Z. Du, H. Dong, F. Zhao, H. Yang, J. Borowicz, Z. Xu, Z. Li, M. Liu, G. He and I. P. Parkin, *Mater. Today*, 2024, **78**, 32-45.
14. K. Wang, H. Zhan, X. X. Liu and X. Sun, *Adv. Funct. Mater.*, 2024, 2418993.
15. L. Lin, Z. Shao, S. Liu, P. Yang, K. Zhu, W. Zhuang, C. Li, G. Guo, W. Wang, G. Hong, B. Wu,

- Q. Zhang and Y. Yao, *Angew. Chem. Int. Ed.*, 2025, e202425008.
16. K. Wang, Y. Luo, H. Zhan, X. X. Liu and X. Sun, *ACS Nano*, 2024, **18**, 27672-27682.
  17. A. Wu, S. Zhang, Q. Li, W. Xue, C. Li, B. Xi, W. Mao, K. Bao and S. Xiong, *Adv. Energy Mater.*, 2025, 2404450.
  18. R. Chen, Y. Zhong, P. Jiang, H. Tang, F. Guo, Y. Dai, J. Chen, J. Wang, J. Liu, S. Wei, W. Zhang, W. Zong, F. Zhao, J. Zhang, Z. Guo, X. Wang and G. He, *Adv. Mater.*, 2025, 2412790.
  19. K. Wang, H. Zhan, W. Su, X.-X. Liu and X. Sun, *Energy Environ. Sci.*, 2025, **18**, 1398-1407.
  20. B. Ren, X. Zhang, H. Wei, J. Jiang, G. Chen, H. Li and Z. Liu, *Adv. Funct. Mater.*, 2024, 2418594.
  21. S. Zhang, H. Ao, J. Dong, D. Wang, C. Wang, X. Xu, Z. Hou and J. Yang, *Angew. Chem. Int. Ed.*, 2025, **64**, e202414702.
  22. Y. Pan, Z. Zuo, Y. Jiao and P. Wu, *Adv. Mater.*, 2024, **36**, e2314144.
  23. R. Jiang, T. Naren, Y. Chen, Z. Chen, C. Zhang, Y. Xie, L. Chen, Y. Qi, Q. Meng, W. Wei and L. Zhou, *Adv. Funct. Mater.*, 2024, **34**, 2411477.
  24. Z. Luo, Y. Xia, S. Chen, X. Wu, E. Akinlabi, B. B. Xu, H. Pan, M. Yan and Y. Jiang, *Energy Environ. Sci.*, 2024, **17**, 6787-6798.